INTERNAL REPORT SDL-90-06

CHARACTERIZATION OF THE WSU SHOCK DYNAMICS LABORATORY'S TIME RESOLVED RAMAN SPECTROSCOPY SYSTEM

R. GUSTAVSEN

September 1990

Shock Dynamics Laboratory
Department of Physics
Washington State University
Pullman, WA 99164-2814

I Overall configuration

This report discusses the collection efficiency of the time resolved Raman spectroscopy system developed at the WSU Shock Dynamics Laboratory. The overall configuration, shown in Figure 1, uses a flashlamp pumped dye laser (Candela SLL 5000) whose energy is delivered to the sample using optical fibers. The Raman signal is also collected into an optical fiber which delivers it to a 0.6 m spectrograph (The final stage of a SPEX Model 1877 "Triplemate"). An electronic streak camera (Hadland Imacon 790) time disperses the spectrum. The image at the streak camera output, intensity vs. wavelength vs. time is amplified using a microchannel plate image intensifier (ITT F4113) and recorded using an intensified vidicon detector (EG&G 1254) and optical multichannel analyzer (OMA).

Unlike previous experimenters who used lens and mirror optics,[1-3] we used optical fibers because they allow lasers, targets and detection equipment to be aligned independently. The target incorporates the sample, the lenses, and fittings for the optical fiber. It can be aligned remote from the gas gun using only a helium-neon (He-Ne) laser and a microscope. A great deal of setup time is therefore saved. Furthermore, the fiber which delivers energy from the laser "homogenizes" nonuniformities in the dye laser beam profile. This is important because "hot-spots" in the beam can damage samples and also make it impossible to estimate the intensity at the sample.

We chose the 45 degree scattering geometry because it minimizes the collection of elastically scattered light. This is important for two reasons; First, most of the Raman signal generated in the fused silica fiber is not collected. We can obtain fine Raman signals from alpha quartz, whose 465 cm^{-1} Raman line is directly on top of the fused silica Raman band. Second, because the amount of collected light at the laser wavelength is small, we don't need filters but can use a single stage spectrograph and thus achieve high throughput. The laser light must be physically blocked, however from entering the streak camera. (A piece of tape over a portion of the time slit is all that is necessary to block the Rayleigh line.)

Section II of this report describes a practical characterization of the system which allows you to estimate the amount of signal you will receive based on the samples scattering cross section and physical thickness, energy in the laser pulse, time resolution and slit widths. Appendix A provides more detailed analysis by estimating the losses and gains of system elements such as the spectrograph or streak camera. Appendix B contains details of target construction including technical drawings and component specifications.

II Experimental characterization of the signal collection efficiency

This section contains the results of calculations and measurements which allow prediction of the amount of signal which can be obtained using a given material, sample thickness, time resolution, spectral slit width, and laser energy.

The instantaneous Raman power collected into the detector is[4]

$$P = \eta_o \int_V \int_\Omega dV d\Omega \frac{d\sigma}{d\Omega} I_L N . \qquad (1)$$

In Eq. (1), V is the volume intersected by the sample, the laser beam, and the collection optics. Ω is the solid angle of collection, and $d\sigma/d\Omega$ the scattering cross section per molecule. I_L is the laser intensity and N is the number density of scatterers in the interaction volume. η_o is the lumped efficiency of the optical collection and recording system. We assume that the the laser intensity, the number density of scatterers, and the scattering cross section, are all uniform within the interaction volume. The sample we consider to radiate uniformly into 4π sr. Thus

$$P = \eta_o N \frac{d\sigma}{d\Omega} I_L \int_\Omega \int_V dV d\Omega. \qquad (2)$$

We now compute Ω, the solid angle for light collection. If an amount of light proportional to Ω_L, the solid angle of the lens, is collected it will be reduced by the factor $\eta = \Omega_F/\Omega_L$ upon entering the fiber. The amount of light entering the fiber will thus be proportional to Ω_F. Similarly the amount of light entering the spectrograph will be reduced by the factor $\eta = \Omega_S/\Omega_F$ so that the amount of light collected is ultimately determined by Ω_S, the solid angle of acceptance of the spectrograph.

The light cone or solid acceptance angle of the spectrograph is limited by the 69 mm diameter square grating and the 600 mm focal length which result in an effective aperture of f/7.7. f/7.7 light has a cone with a half angle of 3.7°, therefore

$$\Omega = \int_0^{2\pi} d\phi \int_0^{3.7^\circ} d\vartheta \sin\vartheta = 2\pi(1 - \cos 3.7^\circ) = .0131 \text{ sr}, \tag{3}$$

and

$$P = .0131 \text{ sr } \eta_0 \frac{d\sigma}{d\Omega} I_L N \int dV. \tag{4}$$

We now compute the interaction volume, V. 1:1 imaging is used between one fiber end and the sample and between the other fiber end and the spectrograph. While an amount of light proportional to A_F, the cross sectional area of the fiber is collected, this amount is reduced by the factor $\eta = A_S/A_F$ upon passing the spectrograph slits which have a clear area A_S. The effective cross sectional area of interaction is thus determined by the spectral slit width, w, and the time slit height, h. The interaction volume is then

$$\int dV = whd\ , \tag{5}$$

where d is the sample thickness, and the instantaneous power is now

$$P = \eta_0 \frac{d\sigma}{d\Omega} I_L N whd\ .0131 \text{ sr}\ . \tag{6}$$

Two parameters can be used to estimate the intensity, I_L, emitted from the fiber connected to the laser. These are the pulse energy, E, and the full width at half maximum of the pulse, T. The laser intensity has a gaussian temporal profile

$$I_L = I_0 \exp\left(- 2.77 \left(\frac{t}{T}\right)^2 \right), \tag{7}$$

where I_0 is the peak intensity. The energy in the pulse is the integral over the time and area covered by the pulse. Hence

$$E = A_F \sqrt{\frac{\pi}{2.77}} I_0 T = 1.065\ A_F I_0 T \tag{8}$$

where A_F is the cross sectional area of the fiber. The intensity of the laser light emitted from the fiber is then

$$I_L = \frac{E}{1.065 A_F T} \exp\left(- 2.77 \left(\frac{t}{T}\right)^2 \right). \tag{9}$$

Laser light is delivered from the fiber tip to the sample using 1:1 imaging. Thus the intensities at the fiber tip and sample differ only because of the reflective losses of the lenses and sapphire window. These losses can be included in the efficiency factor η_0. The instantaneous power delivered to the detector is now

$$P = \eta_0 \frac{d\sigma}{d\Omega} \frac{E}{1.065 A_F T} \exp\left(- 2.77 \left(\frac{t}{T}\right)^2 \right) \text{Nwhd .0131 sr}. \tag{10}$$

The present detection system, consisting of a streak camera, image intensifier and vidicon detector, ultimately integrates signal over a period of time $\Delta\tau$, which is short compared to the laser pulse length. The measured signal S, is thus approximately

$$S = P\Delta\tau = \eta_0 \frac{d\sigma}{d\Omega} \frac{E}{1.065 A_F T} \exp\left(- 2.77 \left(\frac{t}{T}\right)^2 \right) \text{Nwhd } \Delta\tau \text{ .0131 sr} \tag{11}$$

By making a Raman measurement on a particular material we can estimate the system efficiency factor η_0. Because its scattering cross section is well known, and because of our interest in the shocked material, we will use carbon disulfide (CS_2) for this example. Our measurement used the following variables:

1) $\frac{d\sigma}{d\Omega} = 3.3(10^{-29})$ cm^2/molecule-sr
   This is the cross section for liquid CS_2's symmetric stretch 656 cm^{-1} mode when 514.5 nm laser light is used.
2) E, the measured energy in the laser pulse was 40 mJ.
3) T, the FWHM of the pulse was 1.5μs.
4) A_F, the area of the 400μm diameter fiber core is $1.257(10^{-3})$ cm^2
5) N = (10^{22}) molecules/cm^3. This is based on the liquid CS_2 density of 1.26 g/cm^3.
6) w, the width of the spectral slit was 150 μm or $1.5(10^{-2})$ cm
7) h, the height of the time slit was 400 μm or $4(10^{-2})$ cm
8) d, the sample thickness was 200μm or $2(10^{-2})$ cm
9) $\Delta\tau$, the sampling time was 50 ns

Figure 2 shows the Raman signal collected at the peak of the laser pulse (t = 0). This signal is approximately 700 counts high with a FWHM of 10 channels. The most useful efficiency factor, which we shall call η_0, is the one for the peak. From the data above and Eq. 12 we can make an estimate of η_0.

$$700 \frac{\text{counts}}{50 \text{ ns}} = 14 \frac{\text{counts}}{\text{ns}} = \eta_0 \, 1.033 \left(10^{-15}\right) \frac{\text{J}}{\text{ns}} \text{, or}$$

$$\eta_0 = 1.36 \left(10^{16}\right) \text{counts/J} \,. \qquad (12)$$

η_0 was checked in a different cell with a different thickness using various liquids with different cross sections. The number above appears to be a lower limit, because the other measurements indicate that $\eta_0 = 3.6 \pm .3$ (10^{16}) counts/J. As expected, if the same cell, laser energy, ete. were used, the number of counts measured was always proportional to the material's scattering cross section, indicating that non-linear effects are absent.

Given η_0 and Eq. (11) we have a practical method for determining how many counts to expect based on the material's scattering cross section and thickness, the pulse energy, the time resolution and the slit widths.

Appendix A

Subsystem efficiencies

i delivery losses

Between the tip of the optical fiber and the sample are a matched pair of collimating and refocusing lenses. From Figure 3 (Ref. 6) we see that, at wavelengths near 500 nm, the transmittance of each lens will be about 92%. (The lenses are assumed to be made of BK-7, a common optical glass.) There is also an 8% reflective loss at the sapphire-air interface of the rear window. The delivery efficiency is therefore

$$\eta_d = .92^3 = .78$$

Using Eq. (10) we calculate the intensity at the tip of the 400 μm fiber and the peak of the 1.5 μs 40 mJ laser pulse to be 20 MW/cm^2. Because of the 1:1 imaging, the image of the fiber tip is 400 μm in diameter at the sample. Using the calculated delivery efficiency, the peak intensity at the sample is thus 15.6 MW/cm^2.

ii collection losses

Losses on the way to the spectrograph include:

1) 8% reflective loss at the sapphire-air interface of the rear window
2) The 92% transmission of each of the two collecting lenses.
3) 4% at the fiber entrance
4) 6.7% at the fiber to fiber connector (based on specified .3 dB insertion loss).[7]
5) 6.7% in the fiber (based on a loss of 15 dB/ km and 20 m of fiber.[8]
6) 4% at the fiber exit

The efficiency for transport from the sample to the spectrograph is thus

$$\eta_{1\text{-}6} = \prod_{j=1}^{6} \eta_j = .92^3 \; .96 \; .933^2 \; .96 = .625 \; .$$

iii spectrograph losses

Factors limiting the spectrograph efficiency are:

7) The 92% transmittance of the lenses focusing the output of the fiber onto the slit.
8) The 90% reflectance of each of the two aluminized mirrors. (See Figure 3.[6])
9) The grating efficiency of approximately 63%. This is determined by the 70% efficiency of the grating relative to an aluminum mirror[9] (Figure 4), and the 90% reflectance of the aluminum.
10) The 92% transmittance of the cylindrical lens. The clindrical lens was necessary to correct the spectrograph astigmatism which causes vertically and horizontally oriented objects to focus at different positions. In the spectrograph the astigmatism originates from the spherical mirrors being used off axis.

The total efficiency of the spectrograph is thus:

$$\eta_{7-10} = .92^2 .90^2 .63 .92 = .397$$

A ray diagram shows that all of the light leaving the spectrograph will be collected by the streak camera lens and the spectrum will be reimaged on the photocathode with losses due only to the lens. The camera lens used with the streak camera is made of four air spaced, anti reflection coated lenses. Each anti reflection coated surface will have a loss of approximately 1% so the total lens efficiency will be $.99^8 = .92$.

The total efficiency, from laser delivery to streak camera cathode is then

$$\eta = .78 .625 .397 .92 = .178$$

Using this efficiency in Eq. (4) with the 20 MW/cm^2 peak intensity in the laser pulse and the parameters in the end of section B, we find the peak power falling on the streak camera photocathode to be .185 μW

With 514.5 nm laser light and a Raman shift of 656 cm^{-1}, the energy of the Raman photons is 18,780 cm^{-1}. There are therefore $2.68(10^{18})$ photons/J of Raman energy. The peak Raman power (of .185 μW) is thus equivalent to $4.95(10^{11})$ photons/ second, 495 photons/ ns or $2.47(10^4)$ photons/ 50 ns.

iv streak camera

The calibration curve, Figure 5, for the Imacon 790 streak camera indicates that for every watt of 550 nm photons which fall on the photocathode, 20 mA of photo-electrons are produced. The quantum efficiency of the photo cathode is therefor .047, or approximately 1 in 21 photons produces a photo-electron. We therefore have 24 photo-electrons/ns or 1,180 photo-electrons/ 50 ns (1 OMA track) produced in the streak camera. Because we measured a peak of 700 OMA counts with a FWHM of about 10 counts, we ultimately obtain 7,000 counts. The detection system, from this point onward provides gain enough to produce about 6 counts per streak camera photoelectron

The Imacon manual indicates that the total light gain for the streak camera will be 160 times. This figure is based on a brightness gain of 40 and an area gain of 4 due to the 1:2 magnification. The streak camera output is therefore expected to be $7.9(10^4)$ photons/ ns.

v image intensifier

When the image intensifier is operated at the maximum micro-channel-plate voltage of 700 V, it has a gain of approximately 7,000. (See Figure 6.) We can thus expect an output of $5.5(10^8)$ photons/ns.

Paul Horn[10] estimated that, using a fiber bundle, the coupling efficiency between the image intensifier and the vidicon was about 35%. Our measurements indicate that coupling to the vidicon detector using lenses produces a far better signal to noise ratio, particularly at high gains, compared to fiber optic coupling. In fact, with the fiber bundle coupling, the intensifier could not be run at high gain. The efficiency of the lens coupling is only about 1/4 to 1/5 that of the fiber coupling however so the lens coupling efficiency is probably only about 7%. This means about $3.88(10^7)$ photons/ns will be coupled to the vidicon detector.

vi vidicon detector

The vidicon detector efficiency is .05 counts per photon. (See Figure 5) Because the detector is scanned only once, only about half of the charge is actually available, and the number of counts per photon is therefore ~ .025.[10] Using these numbers, there should be $4.85(10^7)$ count/50ns available. If the spectral width is 10 channels (FWHM) the peak

signal will be $4.85(10^6)$ counts. In practice we get 700 counts so our estimate is high by a factor of 7,000.

The cause of this factor of 7,000 is not known. It cannot be due to collecting 1/7,000 times the number of photons we calculated because this would leave us with only 3.5 photons in each 50 ns time period. 3.5 photons is not enough to produce even one photoelectron. More likely, the system is not nearly as sensitive as the specifications suggest or else I have misunderstood the specifications.

Appendix B

Target construction

A cross sectional view of the target assembly is shown in Figure 7. The sample is attached to the front of a hollowed out disk which threads onto the main target body. Into the main target body two lens holders are threaded. The optics contained in the 45° lens holder collimate laser light emerging from the fiber tip and refocus it onto the sample. The optics in the vertical lens holder collect the light scattered from the sample into the other fiber. The 45 – 90 degree geometry minimizes collection of laser light reflected off the sample surfaces. Because the lens holders and sample mount translate along axes with a common intersection, this design makes it easy to put the foci of the laser delivery and collection optics coincident with the sample.

The spring loaded Belleville washers, which are used as spacers between the target plate and target, allow us to align the sample face perpendicular to the impact axis. The impactor is mounted on a small cylinder attached to the front of the projectile. The 45° hole in this mount allows laser light to escape and, like the open 45° port, helps to minimize collection of elastically scattered light.

Figure 8 is a detailed drawing of the main target body and the hollowed out disk for mounting the sample. (Not shown is a nylon locking screw (typically #6-32), threaded through the side of the sample mounting disk.) Samples of solids such as quartz are mounted directly in the sample mounting disk, or, as shown in Figure 7, attached to a window made of a material such as sapphire. If the Raman signal is collected directly from a thick crystal, it is important to recognize that Raman light will be collected from approximately 1 mm of material, thus limiting the time resolution. If the sample is attached to a window, it is important not to use epoxy in the central area, as the laser will damage the epoxy. With either type of sample, the hole in the center of the sample mounting disk is enlarged to the size of the sample and the sample epoxied in place.

If a liquid sample is used, a brass cell such as those used in the CS_2 absorption experiments[11] can be modified and mounted in the sample mounting disk. The cell modification involves cutting away the back portion of the cell so that a step approximately .050" high is created just behind the fill tubes. The hole in the center of the sample mounting disk is then enlarged to the size of the cut-away portion of the cell, and the cell is either epoxied or soldered in place. With the windows and/or sample installed, the target mounting disk is attached to the target mounting plate (Figure 10) using spring loaded

Belleville washers. The front surface of the sample is aligned parallel to the impact plane using an autocollimator.

Before mounting the lenses in the lens holders (Figure 9), a small hole should be drilled in the top so that the holder can be evacuated. Next mount the first plano convex lens (Rolyn Optics #10.0035, 12.5 mm diameter and 24 mm focal length) in the holder using 5 minute epoxy being careful not to smear the lens. Before this epoxy hardens is also the best time to put in the lens spacing ring.

Now, connect one end of a fiber to a 1 or 2 mW visible laser source. (A small Helium Neon laser works fine.) Thread the other end of this fiber into an OFTI No. 300-4SMA-2211 fiber optic splice. Thread the splice into the 1/4 -36 hole in the top of the lens holder. Place the fiber tip at the focal point of the lens by turning the splice till a sharp image of the fiber tip is projected at infinity. Lock the splice in place with a drop of 5 minute epoxy. After the epoxy has hardened, a very small hole should be drilled through the side of the lens holder so that the volume between the lenses can be evacuated. Finally, mount the second lens in the lens holder.

The target is aligned by using a thin, semi opaque material such as masking or packing tape for a screen on the front surface of the sample. For liquid cells the front window must be removed to do this. Now, connect to the lens holders fibers transmitting light from low power sources (sub mW lasers or light bulbs). Adjust the sample plane of the target so that the 45 and 90 degree beams intersect and then adjust the beams so that they are in focus at the sample plane. After two to four iterations of the step above, the target is aligned and all lock nuts and screws should be tightened making the alignment permanent.

The impactor holder is shown in Figure 11. After the impactor is mounted (typically using epoxy), the impactor is aligned to the projectile by machining the rear surface of the holder parallel to the front surface of the impactor. The best way to align the impactor is to mount the holder in a lathe and reflect light from a small He-Ne laser off the impact surface. Adjust the holder in the lathe till the light reflected from the impactor does not move as the lathe rotates. This impactor holder also makes provision for a small (5mm diameter) concave mirror to be placed behind the impactor thus increasing the amount of light collected.

References

[1] N.C. Holmes, W.J. Nellis, W.B. Graham, and G.E. Walrafen, "Raman spectroscopy of shocked water" in "Shock Waves in Condensed Matter" Edited by Y.M. Gupta, Plenum, New York (1985) pg. 191

[2] C.S. Yoo, Y.M. Gupta, and P.D. Horn "Pressure-induced resonance Raman effect in shocked carbon disulfide" *Chem. Phys. Lett.* **159**(2,3) 178 (1989)

[3] Y.M. Gupta, P.D. Horn, and C.S. Yoo "Time resolved Raman spectrum of shock-compressed diamond" *Appl. Phys. Lett.* **55**(1),33, (1989)

[4] Adapted from Eq. (18.1-4) of A. Yariv "Quantum Electronics 2nd Edition", Wiley, New York (1975) pg. 476

[5] A. Yariv "Quantum Electronics 2nd Edition", Wiley, New York (1975) pg. 478

[6] Melles Griot "Optics Guide 4", Melles Griot Inc. (1988) pg. 3-4

[7] Amphenol corp. Fiber optics SMA data sheet. We use OFTI (Optical Fiber Technology Inc.) connectors, however they conform to SMA standards.

[8] Diaguide Corp. SM400-SY data sheet. The specified loss is 10dB/km at 850 nm.

[9] Optometrics Corp. 1990 Optical Components catalog pg. 3-13

[10] Paul Horn "Time-resolved recording of low intensity optical spectra in dynamic experiments" WSU Shock Dynamics Laboratory internal report No.86-02

[11] C.S. Yoo and Y.M. Gupta *J. Phys. Chem.* **94**(7),2857 (1990)

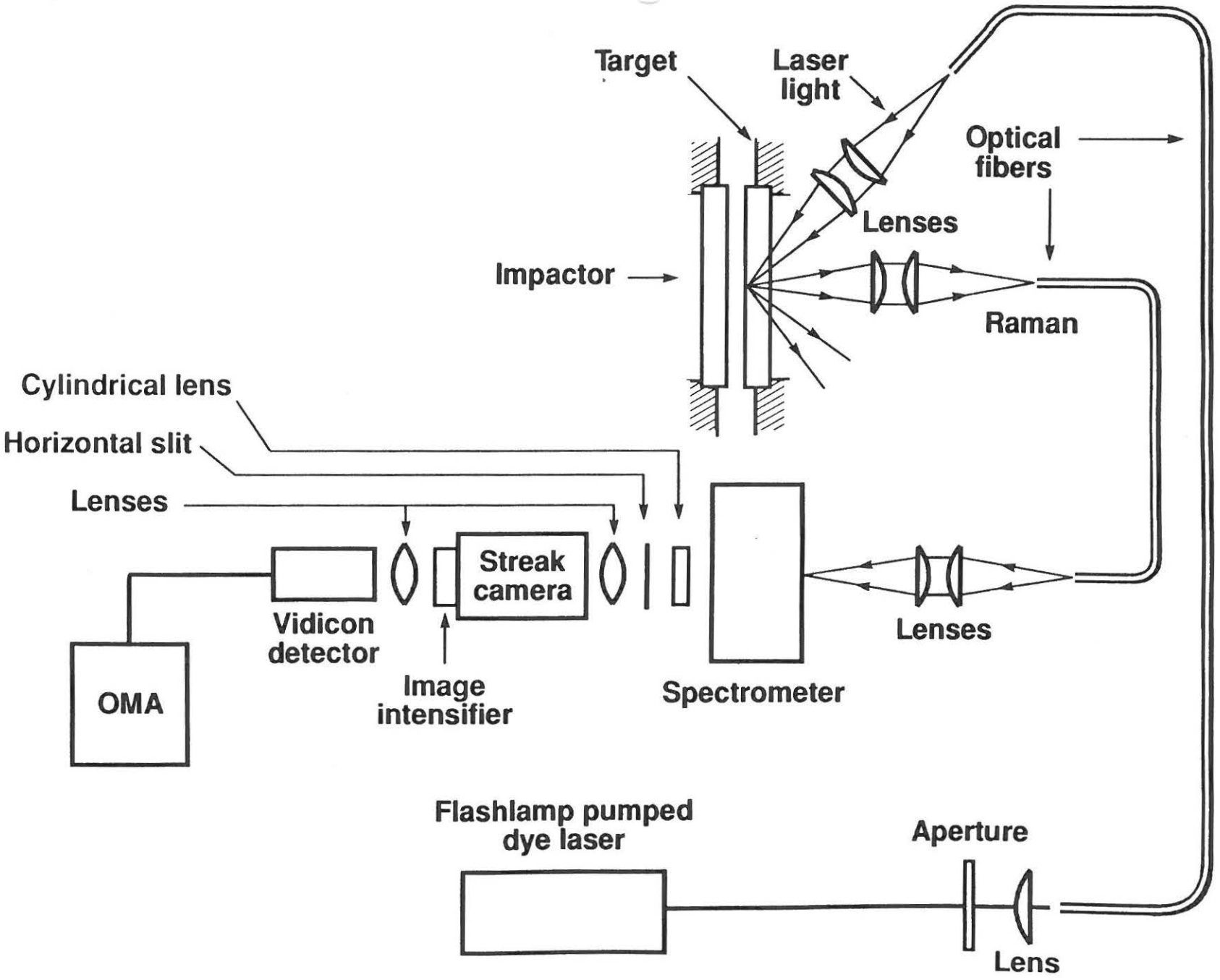
Target
Laser light
Optical fibers
Lenses
Impactor
Raman
Cylindrical lens
Horizontal slit
Lenses
Streak camera
Vidicon detector
OMA
Image intensifier
Spectrometer
Lenses
Flashlamp pumped dye laser
Aperture
Lens

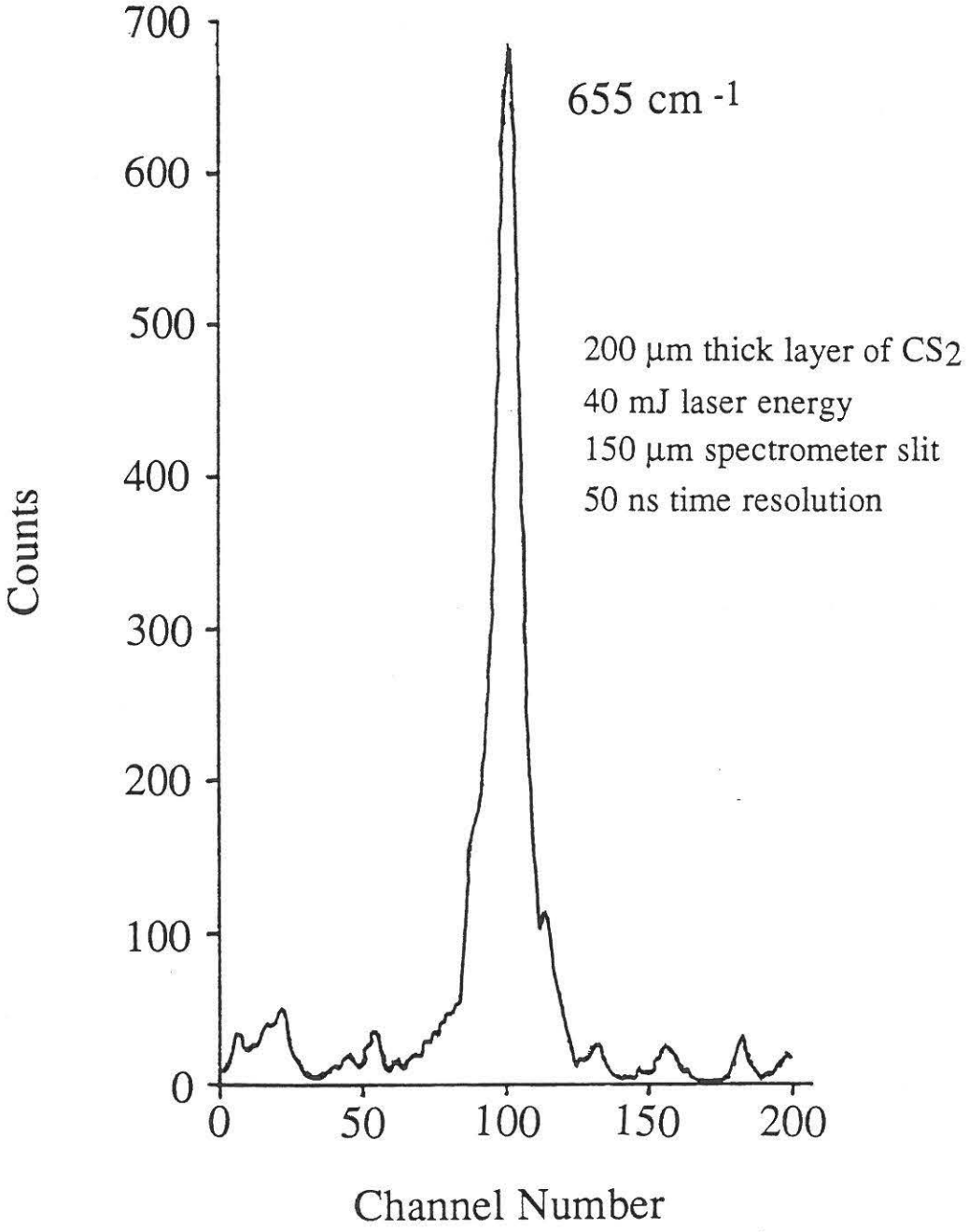

Figure 2 Measured CS_2 spectrum.

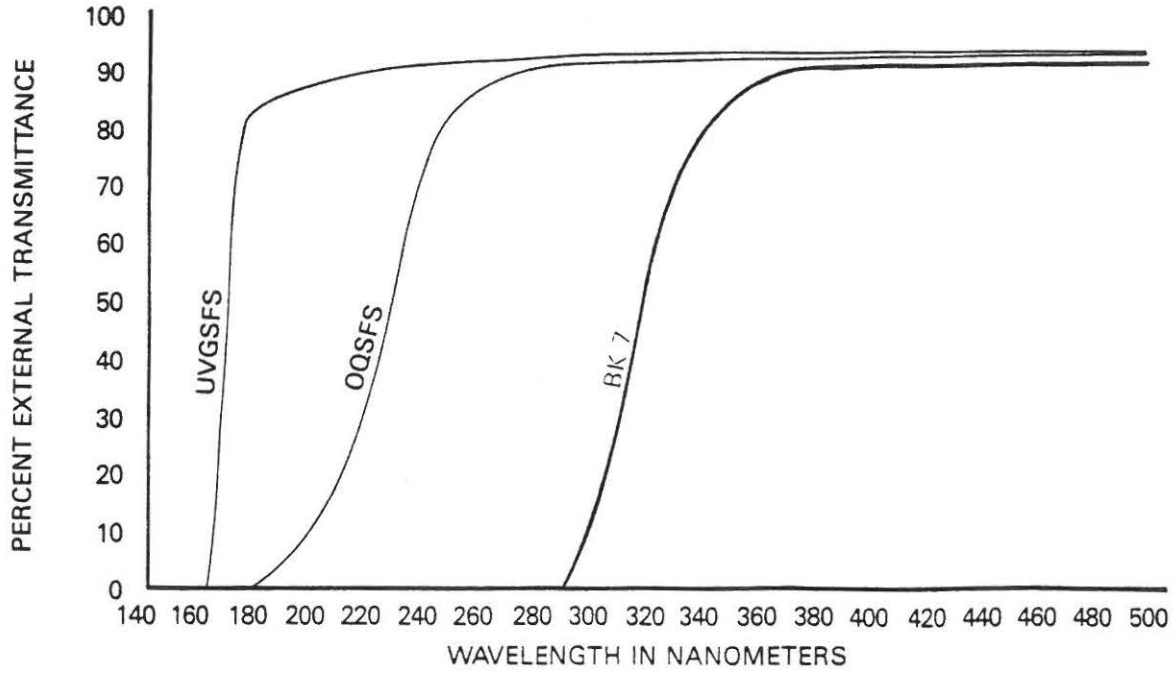

Comparison of external transmittance for uncoated 10 mm thick plates of ultraviolet grade synthetic fused silica (UVGSFS), optical quality synthetic fused silica (OQSFS) and a common optical glass (BK-7).

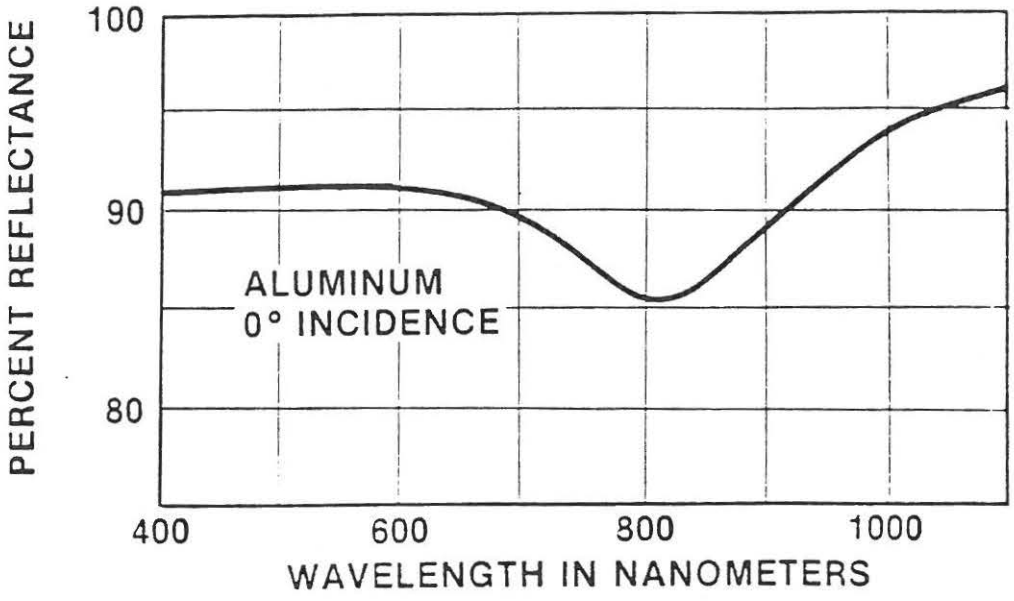

Reflectance of uncoated aluminum.

Figure 3

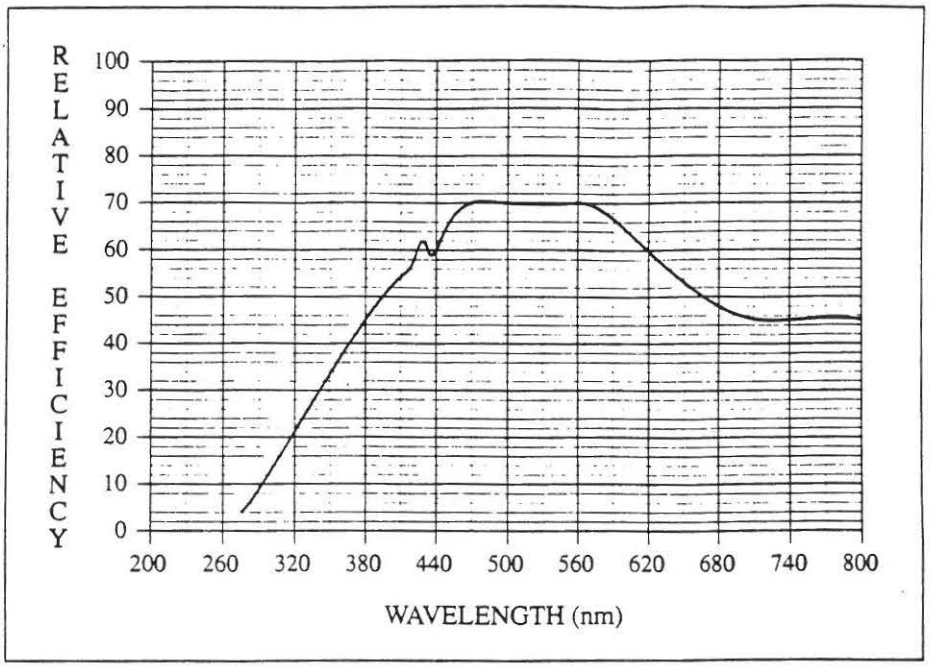

1200 grooves/mm
BLAZED AT 500 nm

Relative efficiency of a 1200 line/mm grating blazed for peak efficiency at 500 nm. The absolute efficiency is calculated by multiplying the relative efficiency by the efficiency of an uncoated aluminum mirror.

Figure 4

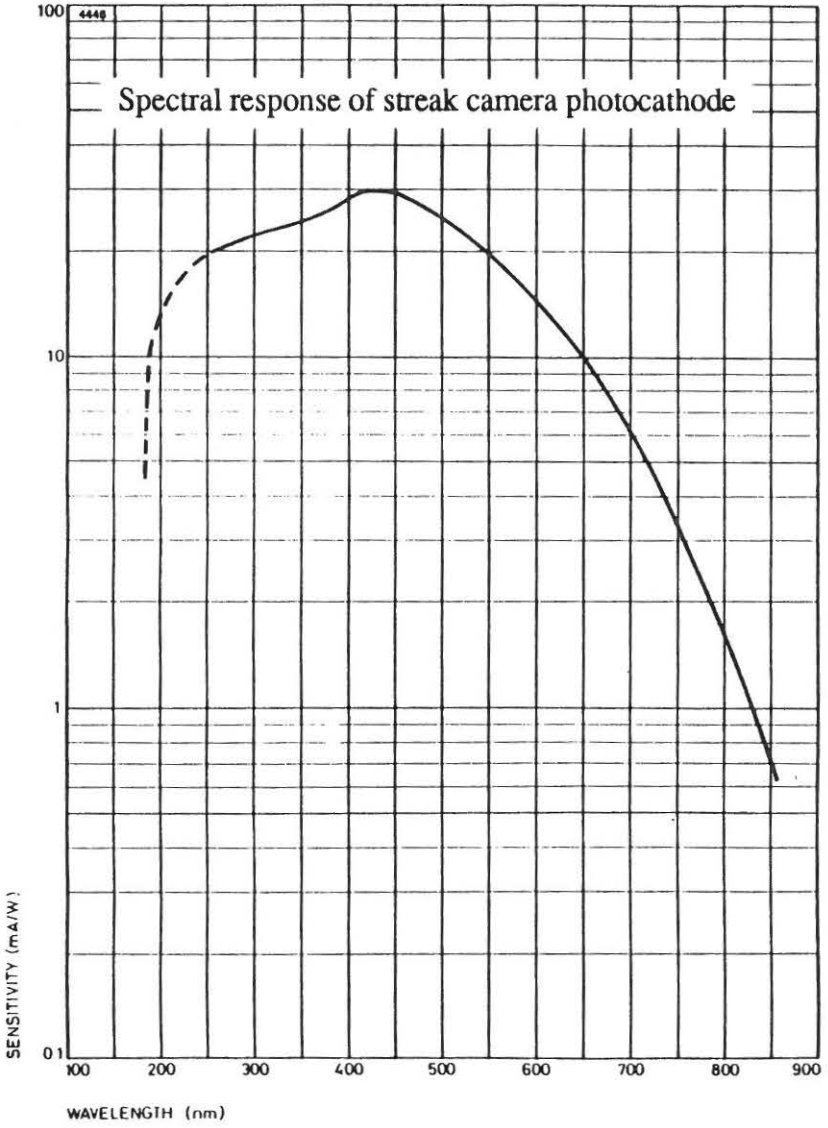
Spectral response of streak camera photocathode
100
10
1
0.1
100
200
300
400
500
600
700
800
900
SENSITIVITY (mA/W)
WAVELENGTH (nm)

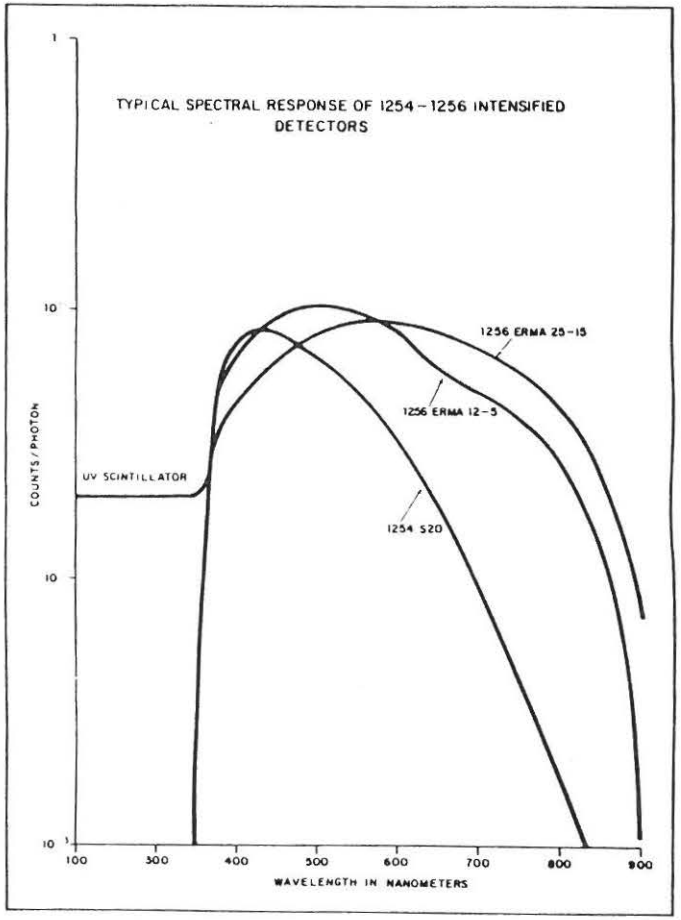
TYPICAL SPECTRAL RESPONSE OF 1254 - 1256 INTENSIFIED DETECTORS
1256 ERMA 25-15
1256 ERMA 12-5
UV SCINTILLATOR
1254 S20
COUNTS / PHOTON
WAVELENGTH IN NANOMETERS

Figure 5

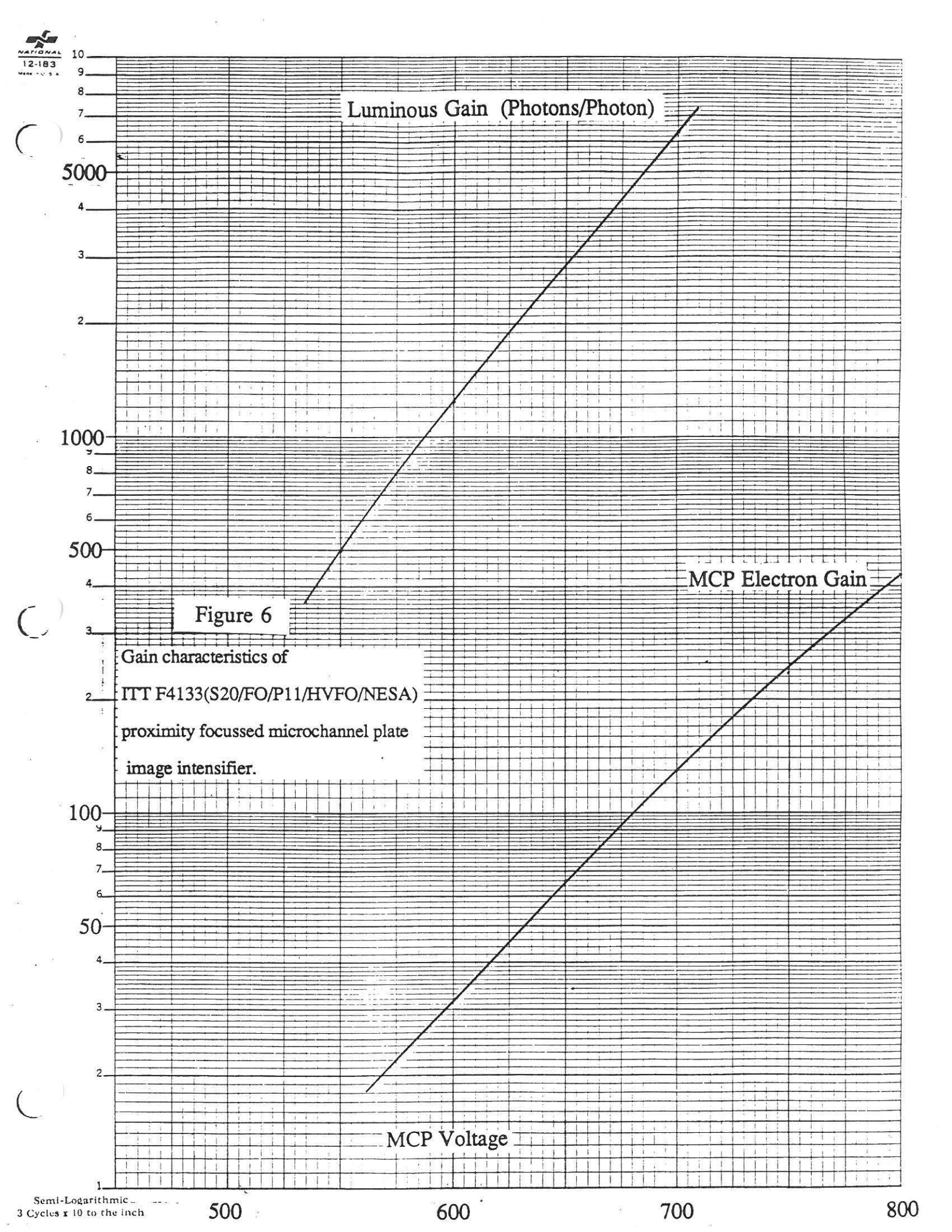

Figure 6

Gain characteristics of ITT F4133(S20/FO/P11/HVFO/NESA) proximity focussed microchannel plate image intensifier.

Semi-Logarithmic
3 Cycles x 10 to the inch

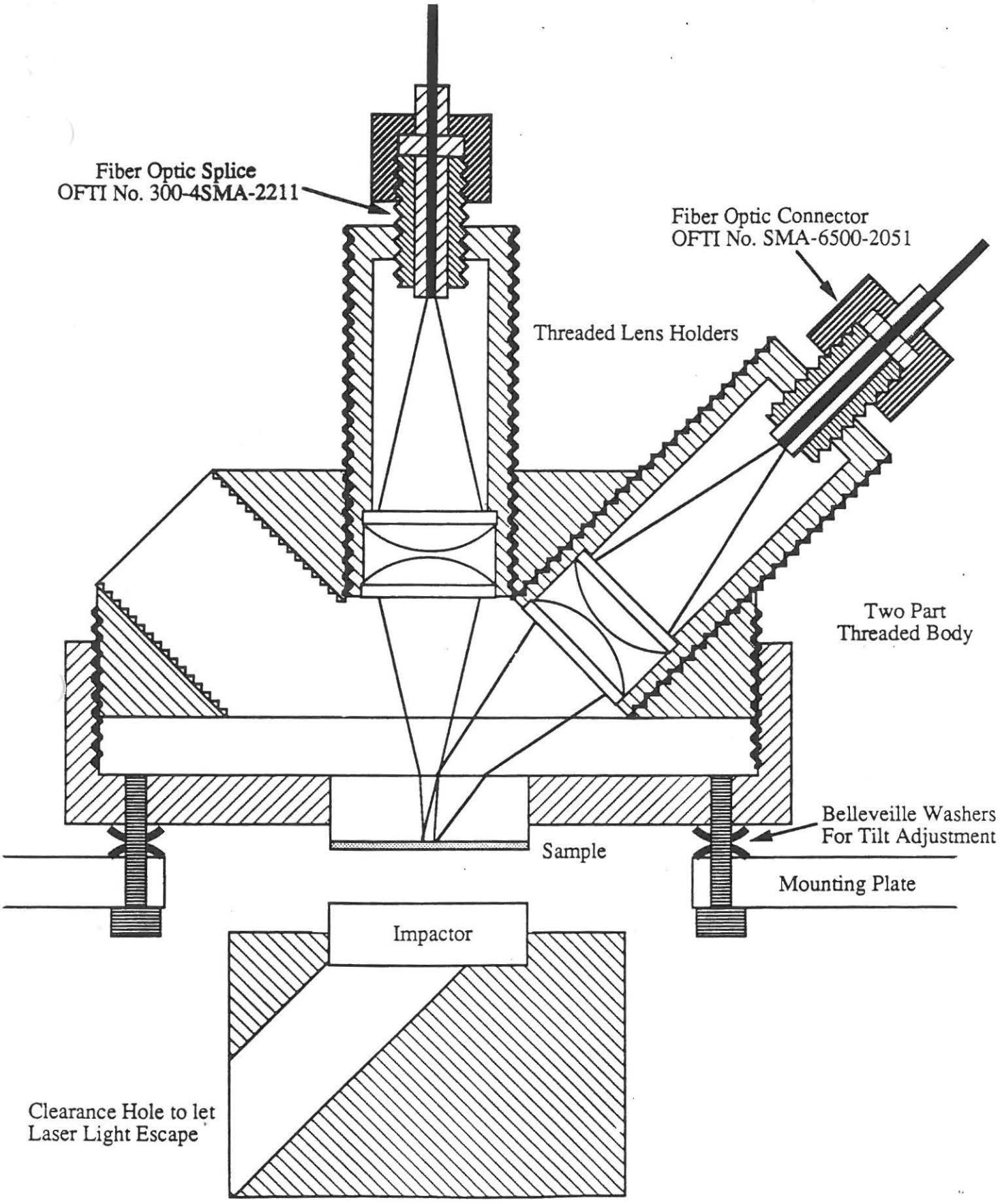

Figure 7 Cross sectional view of target and impactor assembly

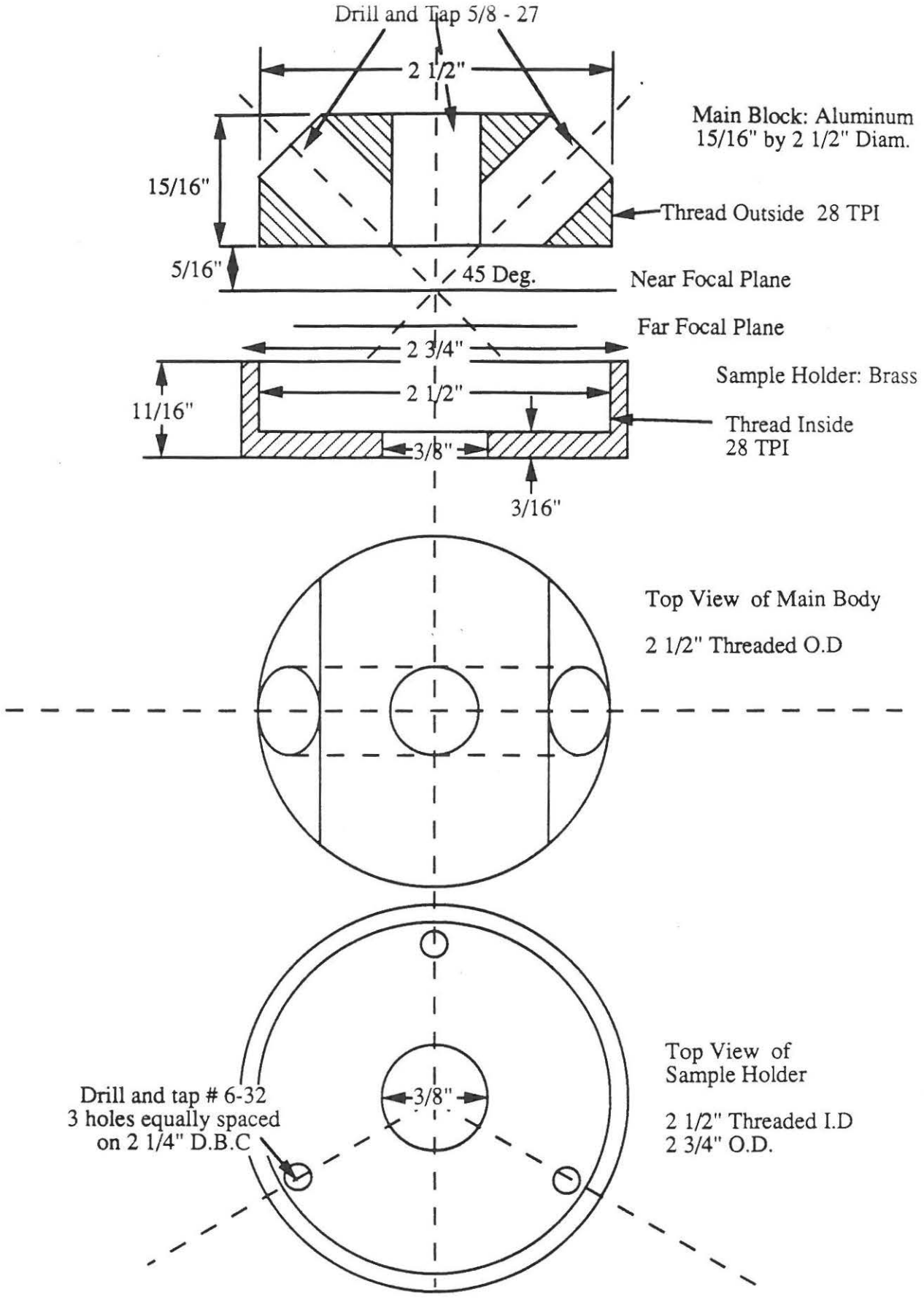

Figure 8 Cross sectional view of target

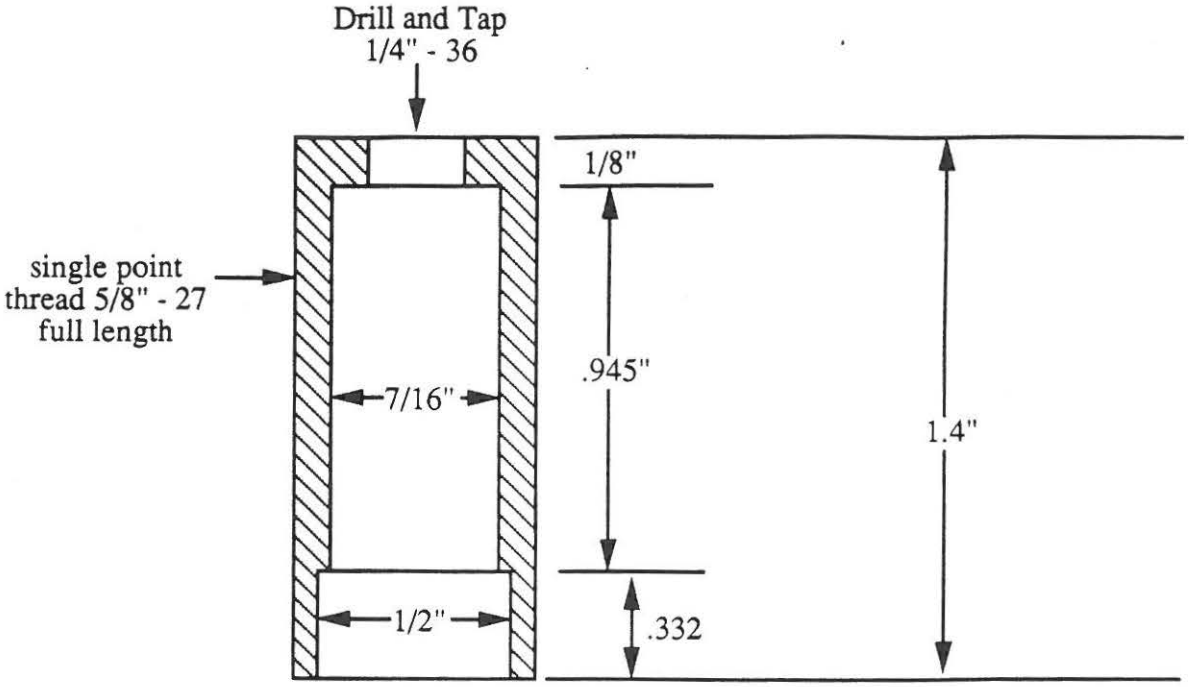

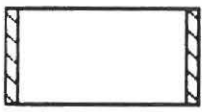

SPACER RING: Material anything
7/16" ID, 1/2" OD, 1/8" Height

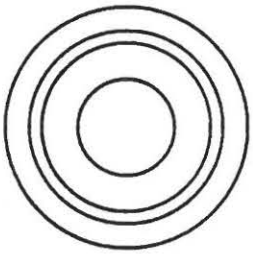

Figure 9 Lens Holder: Material brass. Include lock nuts with each lens holder.

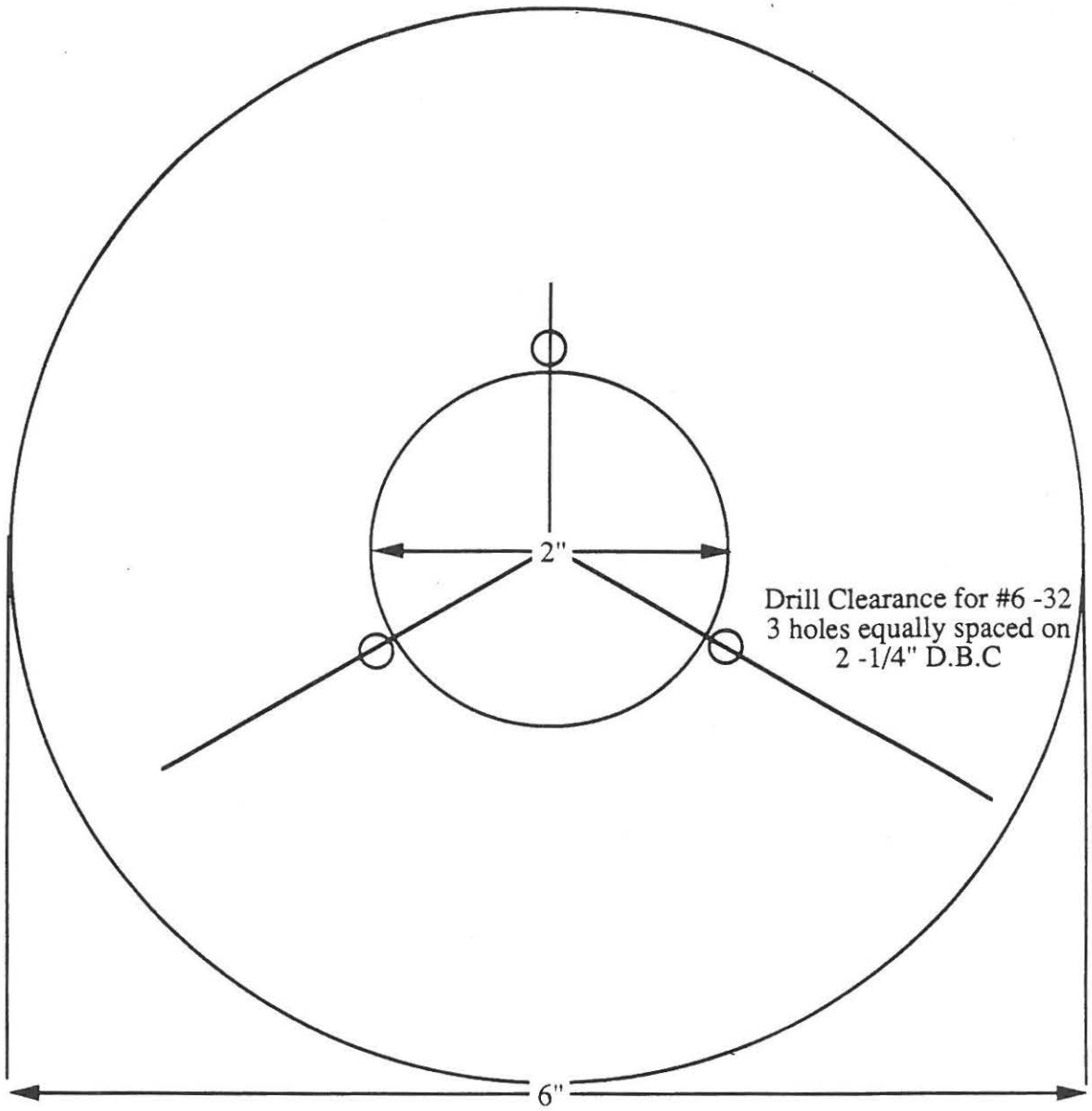

Figure 10 Target mounting plare: Material 3/16" thick aluminum.

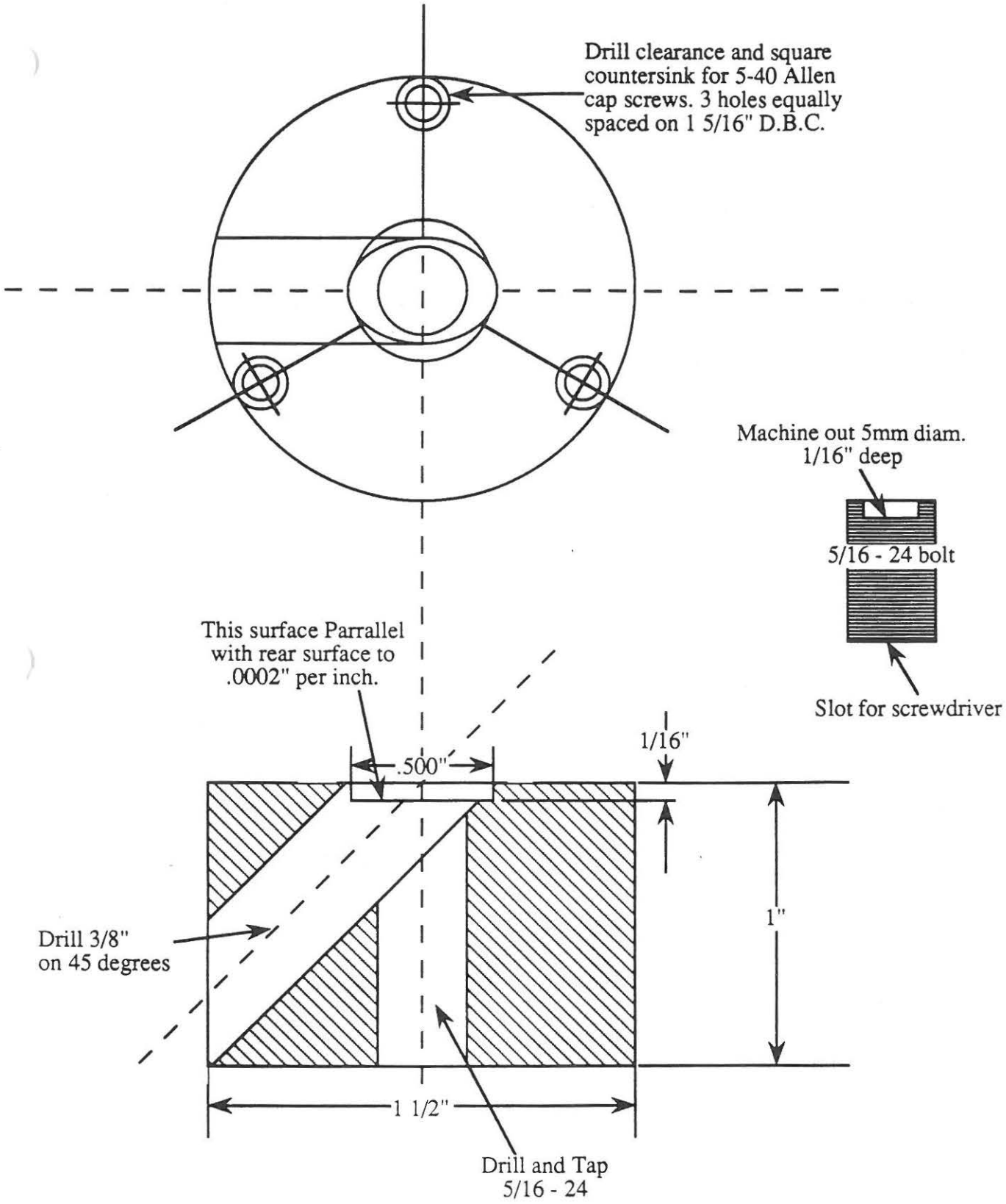

Figure 11 Impactor mount: Material aluminum. The recessed bolt is for an optional 5mm diameter concave mirror.

INTERNAL REPORT SDL-91-01

DETERMINATION OF THE CRYSTAL ORIENTATION OF A PARTICULAR RUBY CRYSTAL

RICHARD L. WEBB

May 1991

Shock Dynamics Laboratory

Department of Physics

Washington State University

Pullman, WA 99164

I. Objective

An r-cut ruby crystal (cut on the (1 $\bar{1}$ 0 2) plane) was ordered from Union Carbide and it was desired to verify that this was indeed the orientation of the crystal. Figure 1, obtained from Union Carbide, shows the orientation of the r-plane with respect to the other major crystal faces. The specific aim of this paper is to verify that the orientation is (1 $\bar{1}$ 0 2), but the paper is written with enough general information that it should be helpful in determining the crystal orientation of any sapphire or ruby crystal.

II. Method

A back-reflection Laue photograph was made of the crystal and used to determine the orientation of the crystal. A back-reflection Laue photograph is made by directing a collimated beam of "white" radiation (usually Bremsstrahlung radiation which covers a large range of wavelengths) through a photographic film (the beam should be normal to the plane of the film) and onto a sample. The allowed reflections are then recorded on the film. The details of how to take a Laue photograph can be read in the manual for the Laue camera and on pages 28-29 of ref. 1. It is recommended that for the Molybdenum target used in our Laue camera, 20 kV at 20 ma be used and the sample set 3 cm from the film. Under these conditions, the Laue photograph of the ruby was completed in ten minutes.

For a reflection to occur from a plane of atoms, the angle of incidence must equal the angle of reflection. Thus each plane can have only one reflection which will make an angle of 2θ with the incident beam where θ is the angle between the normal to the plane and the incident beam. Because of this condition the Laue pattern is very similar to a stereographic projection and possesses the same symmetry (with the added center of symmetry if one does not already exist because the X-ray reflection is the same from either side of a plane) as a stereographic projection.

The first step in determining the crystal orientation from a Laue pattern is to determine the pattern's symmetry. If no symmetry is discernible, it is virtually impossible to

determine the orientation without prior knowledge about the orientation. For sapphire, a trigonal system with the $\bar{3}m1$ point group, the symmetries possible are $3m1$, m, and 2 for the {0 0 0 1}, {h 0 $\bar{h}$ l}, and {1 1 $\bar{2}$ 0} planes respectively.[2] The three-fold rotational symmetry of {0 0 0 1} is easily discernible (although it may be mistaken for six-fold symmetry because of the mirror) as is the two-fold symmetry of {1 1 $\bar{2}$ 0}. If the Laue pattern exhibits only mirror symmetry, the task is a bit more difficult.

In the case of only mirror symmetry, the first thing to do is look at the stereographic projection of sapphire (see Appendix) on one of the equivalent {1 0 $\bar{1}$ 0} planes (Fig. 2 illustrates the (1 $\bar{1}$ 0 0) plane) and identify planes which appear to have the same general pattern. Figure 2 does not include points for planes with disallowed reflections so it is not a true stereographic projection of sapphire. The Laue patterns for the planes which have a similar pattern to the Laue photograph should then be compared to the Laue photograph to determine which one is the correct symmetry.

III. Results

In practice, the Laue photograph cannot look exactly as the ones I have calculated because the intensities of many reflections are so low that they cannot be seen. Also, higher-order planes than the ones calculated may cause reflections not present on the patterns I have constructed. The best method to determine the orientation from the photograph is to study the major lines of reflections present and the spots where lines intersect. From the initial measurements of the photograph from this particular ruby crystal, it was immediately seen that four strong lines intersected at the center of the Laue photograph. Measuring the angles between the line of mirror symmetry (termed the mirror axis for the remainder of this report) and the other major lines, it was determined that one line was perpendicular to the mirror axis, and the other two were $\pm 47^\circ$ from the mirror axis. It was further observed that major intersections occurred on the mirror axis at 3.7 cm from the center in what was marked the m+ direction and 3.3 cm from the center in what was marked the m- direction. Major

intersections also occurred at ± 3.9 cm from the center on the line perpendicular to the mirror axis. A photocopy of the negative (reflections were re-inked in to make them visible on the photocopy) is shown in Figure 3.

By studying the Laue patterns supplemental to this report, it is immediately seen that only the (1 $\bar{1}$ 0 2) pattern bears resemblance to the actual Laue photograph. Further study shows that the major lines are arranged with one line perpendicular to the mirror axis and lines at ±47° from the mirror axis, exactly what the Laue photograph showed. Direct measurement from the calculated Laue pattern places the (2 $\bar{2}$ 0 10) spot at 3.7 cm from the center of the pattern along the mirror axis and the (4 $\bar{4}$ 0 2) spot at 3.2 cm from the center of the pattern in the opposite direction along the mirror axis. The (1 $\bar{2}$ 1 3) and (2 $\bar{1}$ 1 3) spots appear at ± 3.9 cm from the center of the pattern along the line perpendicular to the mirror axis. These points match up very well with those on the photograph, so based on this data, it was determined that the crystal in question was cut on the (1 $\bar{1}$ 0 2) axis.

Appendix - Construction of Stereographic Projections and Laue Patterns

To construct the stereographic projection of a crystal, it is first necessary to construct a set of orthogonal axis. I chose the normals to the (1 $\bar{1}$ 0 0), (1 1 $\bar{2}$ 0), and (0 0 0 1) planes (the [1 $\bar{1}$ 0 0], [1 1 $\bar{2}$ 0], and [0 0 0 1] directions) to be the $\hat{x}$-, $\hat{y}$-, and $\hat{z}$-axis respectively. For hexagonal coordinates,

$$\cos\phi=\frac{[hh'+kk'+\frac{1}{2}(hk'+kh')]a^{*2}+ll'c^{*2}}{\sqrt{Q_{hkl}Q_{h'k'l'}}}$$

where ϕ is the angle between the normals of the $(hk.l)$ and $(h'k'.l')$ planes.[3] (The . replaces the redundant index.) a^* and c^* are the reciprocal lattice spacings ($a^*=\frac{2}{a\sqrt{3}}$ and $c^*=1/c$). Q_{hkl} is the quadratic form ($Q_{hkl}=(h^2+k^2+hk)a^{*2}+l^2c^{*2}$). Using these formulae, $\cos\phi$ was determined between the normal to each plane and each of the three coordinate axes. For each plane, $x_i=\cos\phi_i$ where x_i is the projection of the unit vector normal to the $(hk.l)$ plane onto the $\hat{x}_i$-axis and ϕ_i is the angle between the $\hat{x}_i$-axis and the normal to the plane. Using standard rotation of axis, the x_i may be rotated to any orientation for the stereographic projection. With the coordinates I chose, the stereographic projection of the (1 $\bar{1}$ 0 0) plane was obtained by plotting x_2 against x_3.

Once the data for the stereographic projection has been obtained, making the Laue pattern for the same plane is quite straight forward. First the conditions limiting reflections must be applied to remove all data sets which cannot produce a reflection (this was done before making the stereographic projection for this report). The limiting conditions are[4]:

indices	restrictions
$hkil$	$-h+k+l=3n$
$h\bar{h}0l$	$l=2n$

so all planes which do not meet these conditions are discarded. From the Bragg equation, the angle between the incident beam and the reflection is 2θ where θ is the angle between the incident beam (and thus the normal to the plane for which the Laue pattern is being

constructed) and the normal to the plane contributing a reflection. Thus, using d for the spacing between the film and the sapphire, the new coordinates for the Laue pattern in terms of the coordinates from the stereographic projection (using x and y for the coordinates of the stereographic projection and x' and y' for the coordinates of the Laue pattern):

$$x' = d\tan(2\theta)\frac{x}{\sqrt{x^2+y^2}}$$

$$y' = d\tan(2\theta)\frac{y}{\sqrt{x^2+y^2}}$$

Plotting the new x' against y' will produce the Laue pattern as it should appear on the photograph.

Figure 2 illustrates the stereographic projection of the $(1\ \bar{1}\ 0\ 0)$ plane with the points due to planes with non-allowed reflections omitted. On this figure five planes which exhibit higher order have been labelled along the mirror axis. Five supplemental figures are included at the end showing the Laue patterns for each of these five planes singled out on Figure 2.

References

1. Elizabeth A. Wood; *Crystal Orientation Manual*, (Columbia University Press, New York and London 1963).

2. Norman F.M. Henry and Kathleen Lonsdale, eds.; *International Tables for X-Ray Crystallography*, (Kynoch Press, Birmingham, England 1972) v. 1 p. 40.

3. ibid. v. 2 pp. 112-5.

4. ibid. v. 1 p. 275.

Major Crystal Planes	
Structural indices	Mineralogical symbol
(0 0 $\bar{0}$ 1)	c
{1 0 $\bar{1}$ 0}	m
{1 1 $\bar{2}$ 0}	a
{1 $\bar{1}$ 0 2}	r
{2 $\bar{1}$ $\bar{1}$ 3}	n

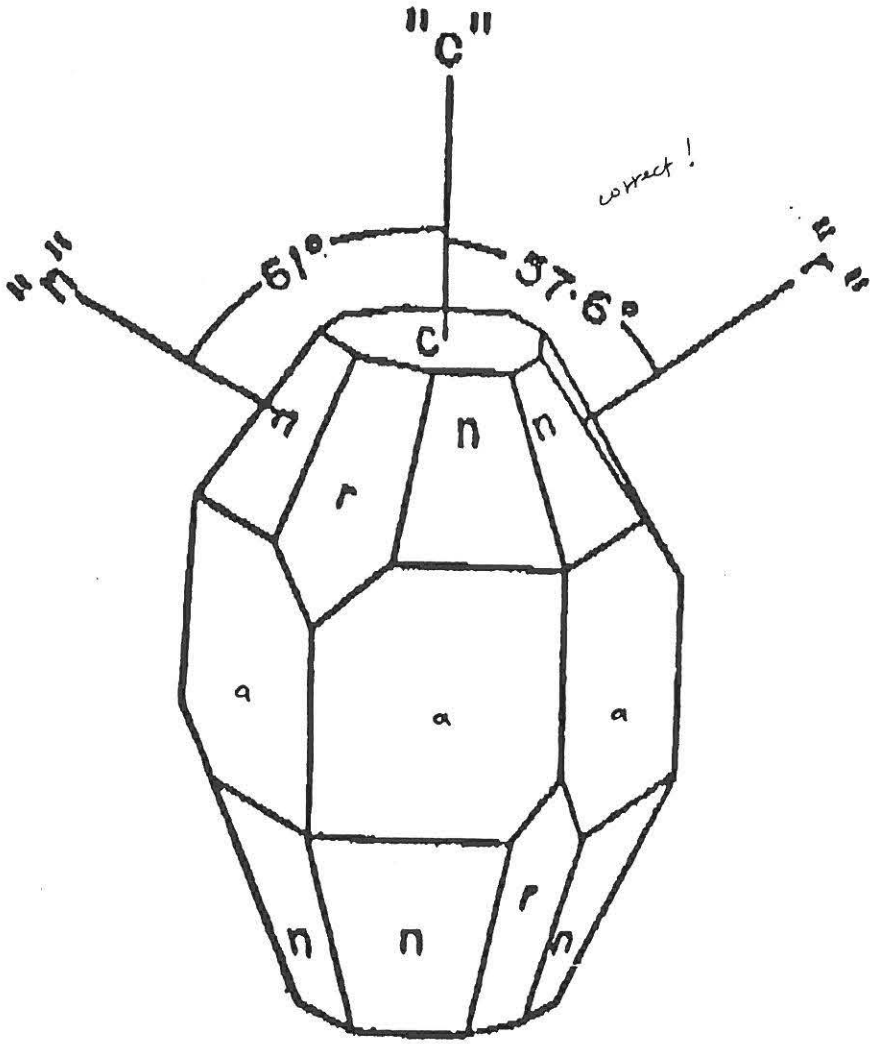

Figure 1 Orientations of the major crystal faces of a hexagonal crystal (such as ruby or sapphire). Figure is provided by Union Carbide.

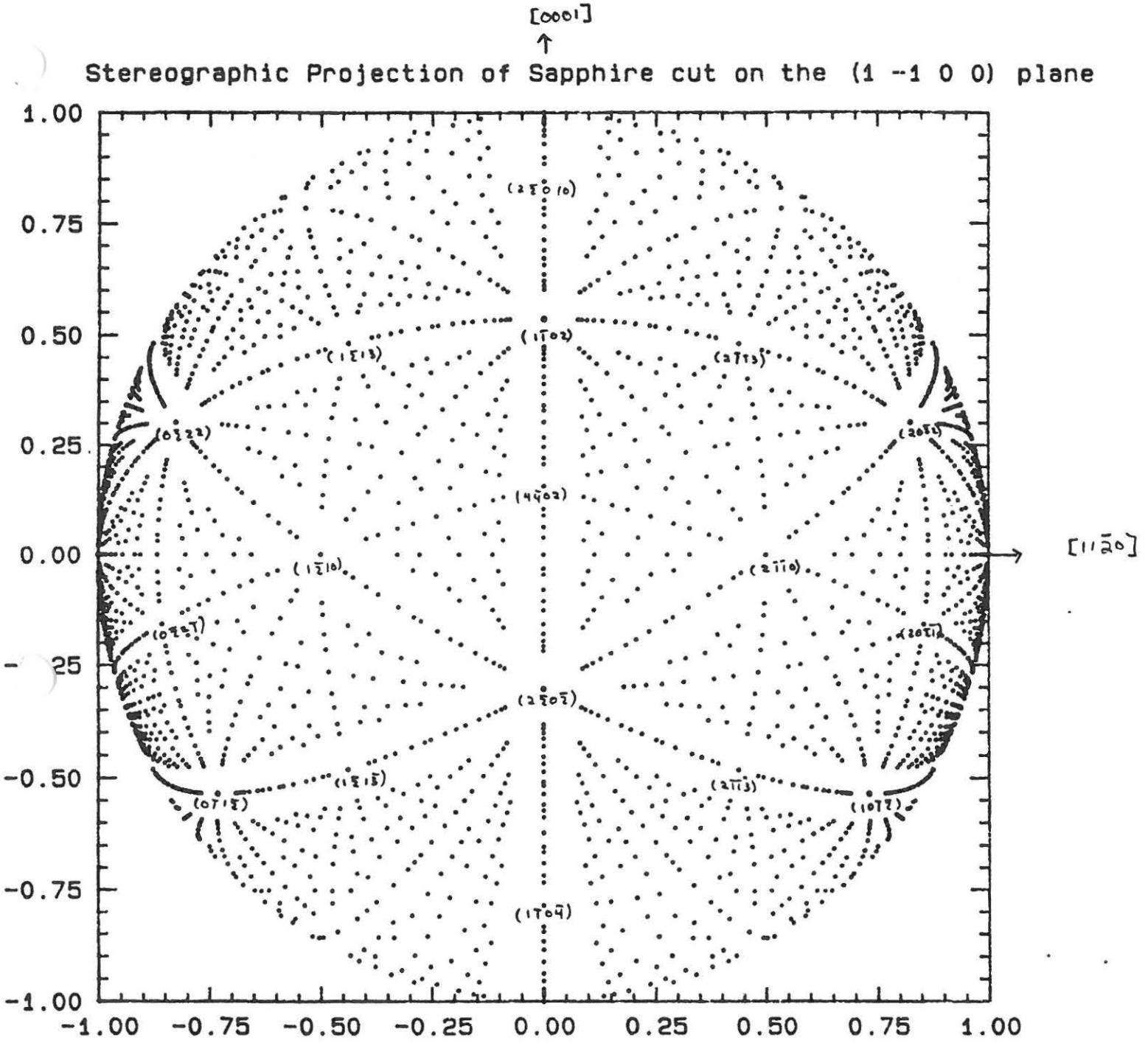

Figure 2 Stereographic projection of sapphire cut on the (1 $\bar{1}$ 0 0) plane with the points due to planes having non-allowed reflections suppressed. The vertical axis is a mirror axis containing planes of the form ($h\ \bar{h}\ 0\ l$). Along this mirror axis, five specific planes have been labeled and the Laue patterns for these planes have been made. Other major planes have also been marked on the figure for reference.

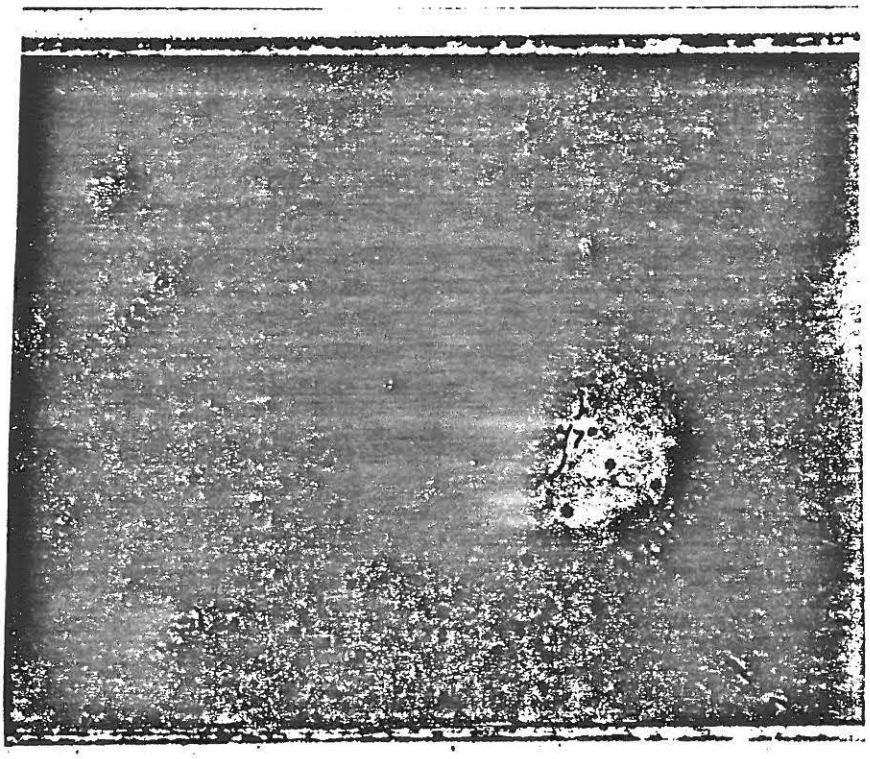

Figure 3 Negative of Laue photograph taken of this particular ruby sample. All reflections visible have been re-inked to make them visible on the photocopy. The four major intersections of major lines have been labeled.

The figure below illustrates all possible reflections in a laue photograph taken of sapphire cut on the (2 $\bar{2}$ 0 10) plane. The figure is scaled for the actual distances on a photograph which was made using a 3 cm separation between the film and the crystal. Some reflections may be so faint that they cannot be seen on the laue photograph. Likewise, a few reflections from higher index planes than this was calculated by may also be present on the photographs. (This was calculated with the parameters $-10 \leq h,k \leq 10$ and $-20 \leq l \leq 20$.)

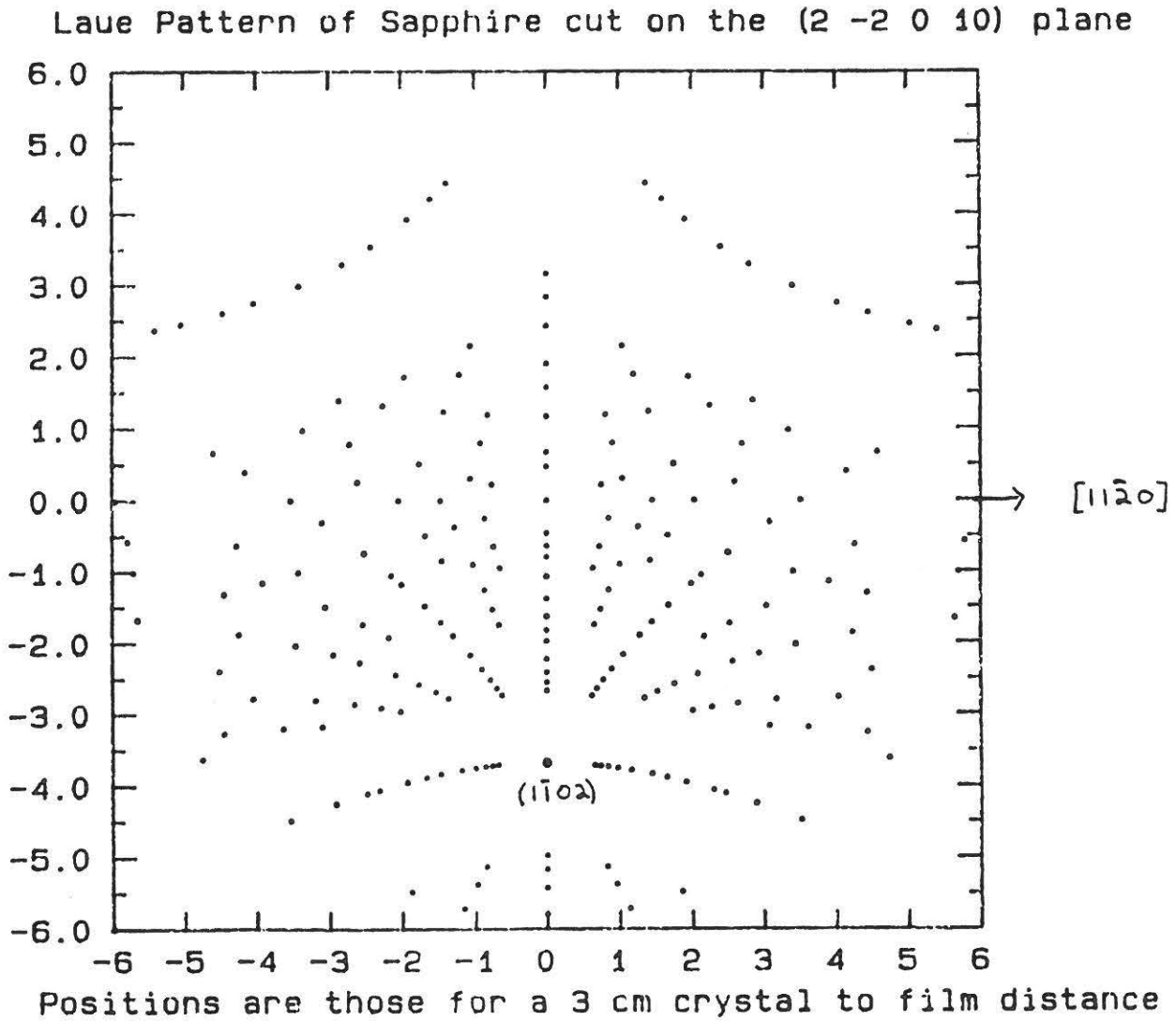

The figure below illustrates all possible reflections in a laue photograph taken of sapphire cut on the (1 $\bar{1}$ 0 2) plane. The figure is scaled for the actual distances on a photograph which was made using a 3 cm separation between the film and the crystal. Some reflections may be so faint that they cannot be seen on the laue photograph. Likewise, a few reflections from higher index planes than this was calculated by may also be present on the photographs. (This was calculated with the parameters -10≤h,k≤10 and -20≤l≤20.)

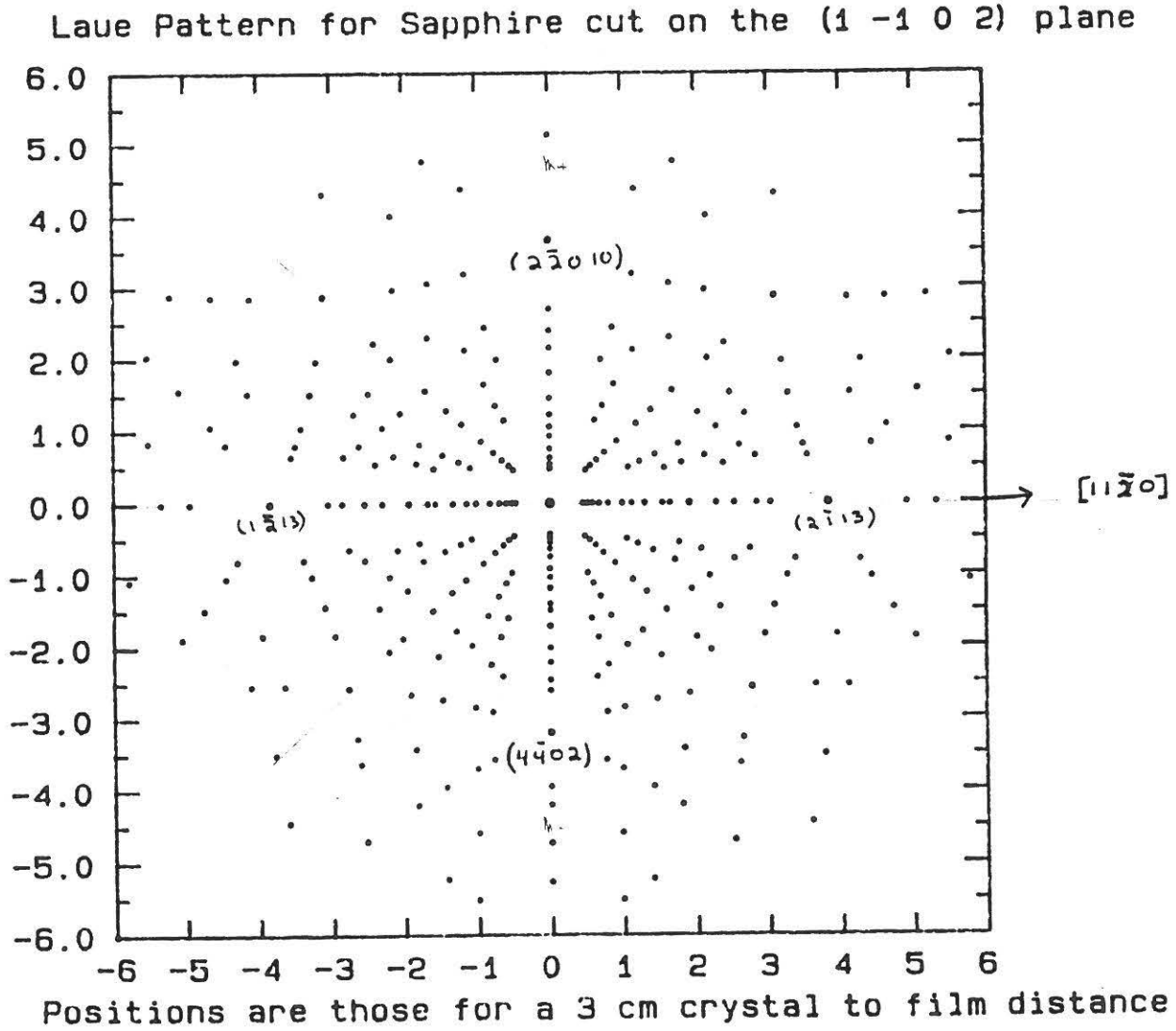

The figure below illustrates all possible reflections in a laue photograph taken of sapphire cut on the (4 $\bar{4}$ 0 2) plane. The figure is scaled for the actual distances on a photograph which was made using a 3 cm separation between the film and the crystal. Some reflections may be so faint that they cannot be seen on the laue photograph. Likewise, a few reflections from higher index planes than this was calculated by may also be present on the photographs. (This was calculated with the parameters $-10 \leq h,k \leq 10$ and $-20 \leq l \leq 20$.)

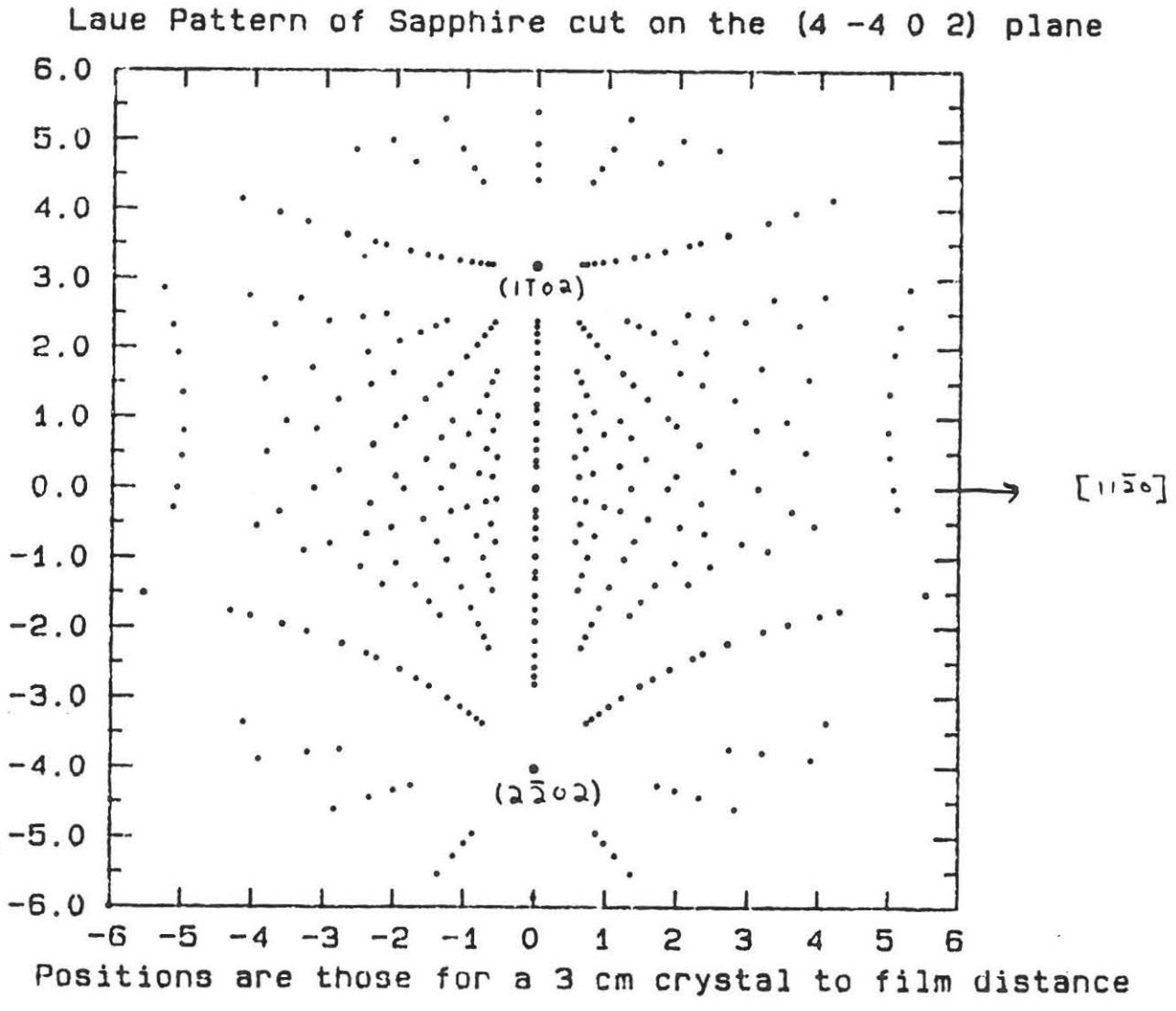

The figure below illustrates all possible reflections in a laue photograph taken of sapphire cut on the $(2\ \bar{2}\ 0\ \bar{2})$ plane. The figure is scaled for the actual distances on a photograph which was made using a 3 cm separation between the film and the crystal. Some reflections may be so faint that they cannot be seen on the laue photograph. Likewise, a few reflections from higher index planes than this was calculated by may also be present on the photographs. (This was calculated with the parameters $-10 \leq h,k \leq 10$ and $-20 \leq l \leq 20$.)

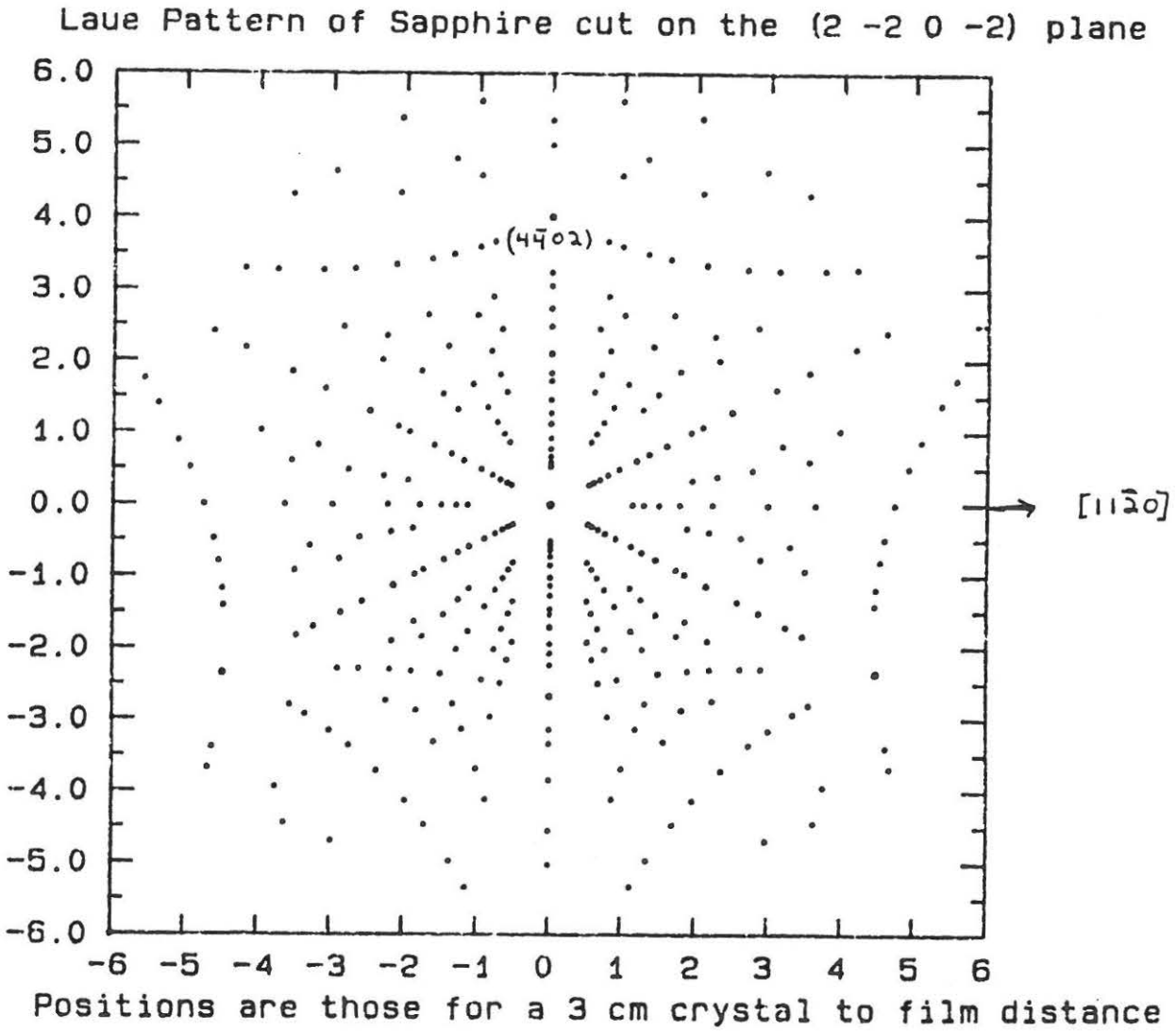

The figure below illustrates all possible reflections in a laue photograph taken of sapphire cut on the $(1\ \bar{1}\ 0\ \bar{4})$ plane. The figure is scaled for the actual distances on a photograph which was made using a 3 cm separation between the film and the crystal. Some reflections may be so faint that they cannot be seen on the laue photograph. Likewise, a few reflections from higher index planes than this was calculated by may also be present on the photographs. (This was calculated with the parameters $-10 \leq h,k \leq 10$ and $-20 \leq l \leq 20$.)

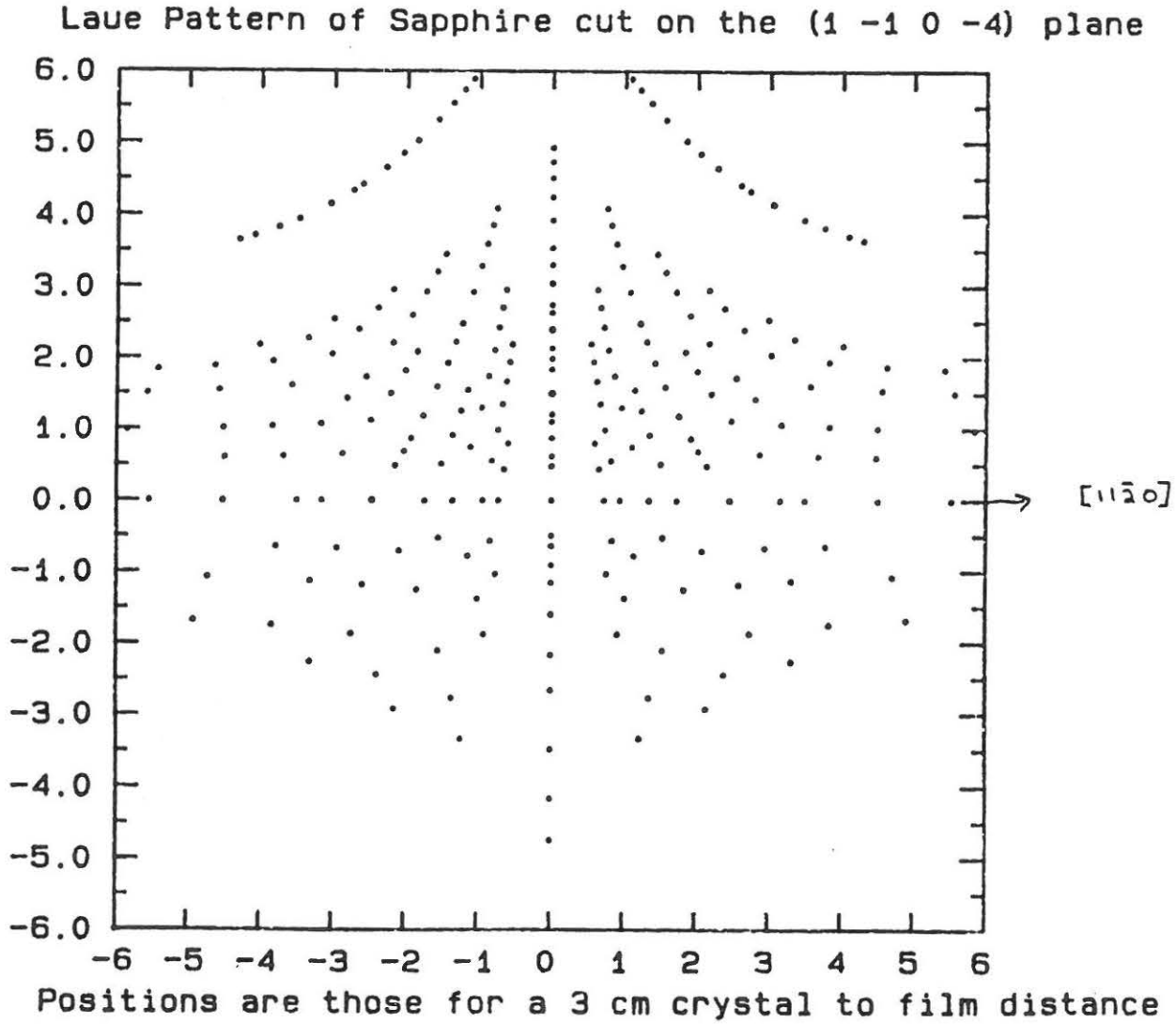

INTERNAL REPORTS - 1991

1. R.L. Webb, "Determination of the Crystal Orientation of a Particluar Ruby Crystal", Internal Report 91-01, May 1991.

2. A. Fanget, "Stability of Numerical Approximations to Time Dependent Flows", Internal Report 91-03, August 1991.